ACS APPLIED MATERIALS & INTERFACES

Research Article

www.acsami.org

Effect of DNA-Induced Corrosion on Passivated Porous Silicon Biosensors

Yiliang Zhao,[†] Jenifer L. Lawrie,[†,∥] Kelsey R. Beavers,[†] Paul E. Laibinis,[†,‡] and Sharon M. Weiss*[,†,§]

[†]Interdisciplinary Graduate Program in Materials Science, [‡]Department of Chemical and Biomolecular Engineering, and [§]Department of Electrical Engineering and Computer Science, Vanderbilt University, Nashville, Tennessee 37235, United States

Supporting Information

ABSTRACT: This work examines the influence of charge density and surface passivation on the DNA-induced corrosion of porous silicon (PSi) waveguides in order to improve PSi biosensor sensitivity, reliability, and reproducibility when exposed to negatively charged DNA molecules. Increasing the concentration of either DNA probes or targets enhances the corrosion process and masks binding events. While passivation of the PSi surface by oxidation and silanization is shown to diminish the corrosion rate and lead to a saturation in the changes by corrosion after about 2 h, complete mitigation can be achieved by replacing the DNA probe molecules with charge-neutral PNA probe molecules. A model to explain the DNA-induced corrosion behavior, consistent with experimental characterization of the PSi through Fourier transform infrared spectroscopy and prism coupling optical measurements, is also introduced.

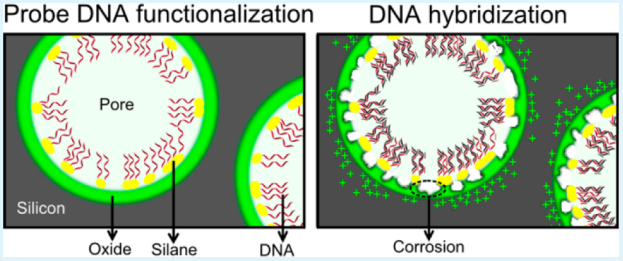

KEYWORDS: *porous silicon, biosensing, waveguide, DNA, PNA, corrosion*

INTRODUCTION

Porous silicon (PSi), a nanostructured material consisting of pores electrochemically etched into a silicon substrate,[1] has attracted considerable interest for potential application in fields ranging from biochemistry[2−5] to photonics[6−8] and solid-state electronics.[9−12] Since PSi was first used as a biosensor almost 2 decades ago there has been growing interest in developing PSi optical structures for label-free biomolecule detection.[13−17] There are many advantages to using PSi in biosensing applications, including its ease of fabrication, large internal surface area (>100 m^2/cm^3) available for molecule capture, compatibility with many functionalization chemistries, and capability for size-selective infiltration of target species.[16,18−25] However, a major challenge for PSi biosensors (which also impacts PSi-based electrodes realized in lithium batteries,[11,26] fuel cells,[10] and supercapacitors[27]) is its reactive surface that tends to make its physical structure unstable in water and various electrolytes.[28] Freshly etched PSi surfaces are hydride-terminated and are highly susceptible to oxidization and dissolution. Accordingly, PSi must be robustly passivated to enable reliable and reusable biosensing applications.

Prior reports have focused on the rapid oxidation and hydrolysis (i.e., corrosion) of PSi fabricated from *p*-doped silicon that occurs when the PSi films are exposed to solutions containing negative charges. In particular, hybridization of negatively charged DNA oligonucleotides was shown to accelerate PSi dissolution.[29] It was suggested that the negative charges on the phosphate backbone of DNA attract positively charged carriers in *p*-type silicon to the PSi surface, facilitating nucleophilic attack by water molecules that ultimately leads to PSi dissolution. Importantly, in the work by Steinem et al.,[29] PSi samples were weakly oxidized to produce a surface with a large fraction of Si−OH bonds and some remaining $Si-H_x$ bonds and were then functionalized with a silane molecule and single-stranded DNA. These samples experienced continuous degradation and ultimately structural collapse upon exposure to the complementary DNA sequence; this corrosion occurred at a much faster rate than background dissolution of the functionalized material in a phosphate buffer solution.

In this work, we expand on prior studies to investigate the effect of DNA-induced degradation on PSi samples that are well-passivated with a thermal oxide and silane layer. PSi waveguide structures consisting of a top, low-porosity guiding layer and a bottom, high-porosity cladding layer are utilized to enable highly sensitive optical measurements that quantify material added to the PSi matrix (e.g., chemical or biological molecules attached to the silicon surface) or material removed from the PSi matrix (e.g., due to corrosion). Details regarding the optical measurements are provided in the Experimental Section. Unlike prior reports, a concentration-dependent DNA-induced corrosion effect is observed for both DNA probe and DNA target attachment, and the corrosion process saturates in time. A sufficiently high DNA probe density to cause PSi corrosion is achieved in this work based on an in situ DNA synthesis process utilizing sequential solid-phase phosphoramidite coupling reactions.[30] For practical implementation of

Received: April 29, 2014
Accepted: August 4, 2014
Published: August 4, 2014

   dx.doi.org/10.1021/am502582s | ACS Appl. Mater. Interfaces 2014, 6, 13510−13519

PSi structures for DNA detection, we show that charge-neutral peptide nucleic acid (PNA) probe molecules can be used to capture the desired target DNA molecules without a confounding corrosion effect. Finally, with supporting Fourier transform infrared spectroscopy (FTIR) measurements, a modified model based on nucleophilic attack of oxidized PSi surface by water molecules is proposed to explain the DNA-induced corrosion process in well-passivated PSi samples.

EXPERIMENTAL SECTION

Materials. All chemicals were of analytical grade and used without further purification. P-type silicon wafers (⟨100⟩, 0.01−0.02 Ω cm, 650−700 μm) were purchased from International Wafer Services, USA. Ethanol, methanol, 4-(2-hydroxyethyl)-1-piperazineethanesulfonic acid (HEPES), KOH, NaOH, HCl, ethylenediaminetetraacetic acid (EDTA), and magnesium chloride hexahydrate ($MgCl_2 \cdot 6H_2O$) were obtained from Fisher Scientific. Hydrofluoric acid (HF) (48−51% solution in water), 3-aminopropyltriethoxysilane (3-APTES), and ethylenediamine (99% extra pure) were purchased from ACROS Organics. NaCl was purchased from EMD Chemicals Inc. *N*-(3-Triethoxysilylpropyl)-4-hydroxybutyramide (TEOS-HBA) was obtained from Gelest. Toluene was purchased from Sigma-Aldrich. 100% complementary DNA target (5′-ACG AGG ACC ATA GCT A-3′) and 100% mismatch DNA target (5′-GGT TTC TGA TGC TGA C-3′) were obtained from Eurofins MWG Operon. Uncharged peptide nucleic acid (PNA) molecules were obtained from BioSynthesis Inc. Deionized (DI) water was produced in-house using a Millipore Elix water purification system and was used in all experiments. DNA synthesis reagents were purchased from Glen Research. Monomers for PNA synthesis, rink amide LL resin, and 2-(6-chloro-1*H*-benzotriazole-1-yl)-1,1,3,3-tetramethylaminium hexafluorophosphate (HCTU) activator were purchased from PNA Bio, EMD Millipore, and ChemPep, respectively.

Fabrication of Porous Silicon Waveguides. The PSi waveguides were fabricated by electrochemical etching of *p*-type silicon wafers (0.01−0.02 Ω cm) in 15% HF acid in ethanol. Before anodization, the silicon wafer samples (2 × 2 cm^2) were first soaked in 15% HF for 1 min to remove the native oxide. The two-layer waveguide structure was then etched at 5 mA/cm^2 for 42 s to form the waveguiding layer and then at 48 mA/cm^2 for 60 s to form the cladding layer. After etching, the samples were soaked in 1.5 mM KOH in ethanol for 30 min to widen pores in order to ease molecule infiltration and attachment. Scanning electron microscope (SEM) images were used to approximate the porosities, pore diameters, and layer thicknesses for these waveguide structures. The resulting PSi waveguide layer has a refractive index of approximately 1.77, pore diameters ranging from 15 to 25 nm, and a thickness of approximately 220 nm. The bottom, cladding layer has slightly larger pore diameters, a refractive index of approximately 1.32, and a thickness of approximately 1400 nm.

Surface Functionalization and in Situ DNA Synthesis. PSi waveguides were first thermally oxidized in a furnace at 800 °C for 30 min. Following oxidation, a hydroxyl-terminated silane, *N*-(3-triethoxysilylpropyl)-4-hydroxybutyramide (TEOS-HBA), was used to functionalize the PSi surface with reactive moieties used to initiate DNA oligonucleotide synthesis from the waveguide surface. In brief, oxidized waveguide samples were incubated in a 4% solution of TEOS-HBA, composed of 83 μL TEOS-HBA, 100 μL DI water, and 1900 μL ethanol, for 4 h. The samples were then rinsed with ethanol to remove excess solvents and annealed at 200 °C for 16 h in an oven. The annealing step cross-links neighboring silane molecules, increasing the hydrolytic stability of the silane coating.[31] Samples were then soaked in DI water at room temperature for at least 4 h to remove weakly bound multilayers of silane molecules.

DNA probes were synthesized within silanized waveguides using an Applied Biosystems model 392 DNA synthesizer that was modified to direct reagent flow onto the waveguide surface for base-by-base oligonucleotide synthesis in PSi. The phosphoramidite method was used as described previously.[30] A dimethoxytrityl (DMT) protecting group is removed following the addition of each base during in situ DNA synthesis. DMT-containing fractions were collected and used for monitoring coupling reactions as described in Supporting Information, Figure S1. Ultramild phosphoramidites and reagents were used to allow for a moderate, basic deprotection step and to reduce the possibility of PSi dissolution during DNA synthesis. A 16-mer probe DNA sequence (5′-TAG CTA TGG TCC TCG T-3′) with a melting temperature of 50 °C in HEPES buffer solution was synthesized. HEPES buffer solution was prepared by dissolving 20 mM HEPES, 150 mM NaCl, and 5 mM EDTA in 1000 mL of DI water. The resulting ionic strength was 110 mM. NaOH or HCl was used to adjust the pH of HEPES buffer to 7.4. After completion of DNA synthesis, the PSi waveguide was rinsed with ethanol and water. Cyanoethyl groups attached to synthesized DNA molecules block the negative charges on the phosphate backbone and need to be removed together with protection groups on each base (phenoxyacetyl protection for adenine, 4-isopropyl-phenoxyacetyl protection for guanine, and acetyl protection for cytosine) before hybridization. Synthesized DNA probe molecules were activated for sensing by deprotection in a 1:1 volume ratio solution of ethylenediamine and ethanol for 30 min.

In Situ PNA Synthesis and Surface Functionalization. Waveguides were first thermally oxidized at 800 °C for 30 min and functionalized with 3-APTES. PSi waveguides were incubated in 1% 3-APTES in anhydrous toluene for 20 min and then rinsed with ethanol to remove excess silane. The silanized waveguides were thermally annealed at 150 °C for 20 min to promote stable 3-APTES monolayer formation and then soaked at room temperature in HEPES buffer for 1 h to remove weakly bound silane multilayers. In situ PNA synthesis of the same 16-mer sequence used for probe DNA (5′-TAG CTA TGG TCC TCG T-3′) was conducted directly on APTES-functionalized PSi within a custom reaction vessel. The synthesis process is described in detail elsewhere.[32]

Nucleic Acid Sensing. 100% complementary target DNA (5′-ACG AGG ACC ATA GCT A-3′) and 100% noncomplementary mismatch DNA (5′-GGT TTC TGA TGC TGA C-3′) were diluted to 100 μM in HEPES buffer and stored at −20 °C. Immediately prior to hybridization, 10 μL of the 100 μM DNA solution was diluted to a working concentration of 10 μM in 90 μL HEPES buffer. PSi waveguides functionalized with either probe DNA or probe PNA were incubated in 100 μL solutions of 10 μM target DNA as well as mismatch DNA. Uncharged PNA molecules with the same sequence as complementary target DNA were utilized to hybridize with PNA probes in order to prevent PSi corrosion associated with negative charges on target DNA. Ten micromolar target PNA solutions were prepared by diluting 100 μM PNA in HEPES buffer. All hybridization experiments were performed at room temperature.

Prism Coupling Measurements. A Metricon 2010 prism coupler employing a rutile prism (n_{prism} = 2.1677) in the Otto configuration was used to evanescently couple a TE polarized 1550 nm laser beam into the waveguide. At a specific resonant angle, the light is coupled through the prism into the waveguide; otherwise, the light is entirely reflected. Therefore, a dip in the reflectance spectrum is observed for each coupled mode. The resonant angle directly corresponds to the effective refractive index of the waveguide according to the relation $n_{eff} = n_{prism} \sin \theta$, where n_{eff} and n_{prism} are the effective index of the waveguide and refractive index of the prism, respectively, and θ is the angle of incidence of light in the prism corresponding to the resonant angle. Molecule infiltration inside the pores of the PSi waveguide causes the refractive index of PSi to increase, leading to a redshift (i.e., shift to higher angle) of the resonant angle. On the contrary, loss of materials inside the PSi waveguide, for example, due to corrosion of the PSi matrix, causes the refractive index to decrease, resulting in a blueshift (i.e., shift to lower angle) of the resonant angle. The magnitude of the resonant angle shift correlates to, and allows quantification of, the amount of material added or removed from the PSi waveguide. When both molecular infiltration and corrosion occur simultaneously, accurate quantification of the respective processes is not possible. Hence, mitigation of the corrosion process is essential for

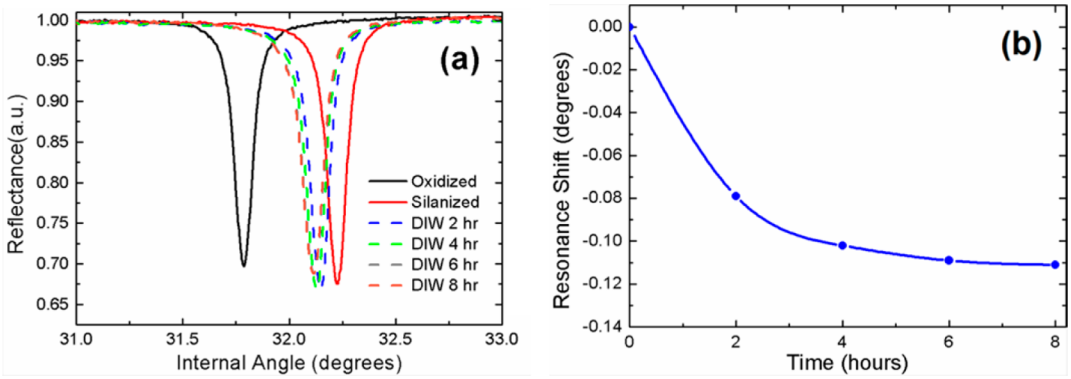

Figure 1. (a) Stabilization of silanized PSi waveguides. Reflectance spectra are given for a PSi waveguide after oxidation (black, solid line), TEOS-HBA silanization (red, solid line), and soaking in DI water for 2, 4, 6, or 8 h (blue, green, gray, orange dashed lines, respectively). Hydrolysis is indicated by shifts of the resonance to lower angles after soaking in DI water. (b) Resonance angle shift as a function of time during DI water soak.

accurate quantification of molecular binding events. The resolution of the Metricon 2010 prism coupler used in this work is 0.002°.

FTIR Characterization. FTIR measurements were performed on a Tensor 27 FTIR spectrometer (Bruker Optics Inc.) with the Seagull variable angle reflection accessory (Harrick Scientific Products Inc.). Reflectance spectra were collected in 64 scans and recorded over a range of 400−4000 cm^{-1} at a resolution of 2 cm^{-1}. All measurements were taken in a nitrogen-purged compartment at room temperature, and an unetched, nonfunctionalized clean silicon wafer was used for background subtraction.

RESULTS AND DISCUSSION

PSi Passivation and Functionalization. The degree of passivation of the PSi waveguides after thermal oxidation and silanization in TEOS-HBA was first established through prism coupling measurements following exposure to an aqueous environment. Thermal oxidation produces a SiO_2 layer and Si−O−Si bonds, leaving the PSi surface free of hydrides and thus less susceptible to corrosion in aqueous environments. The oxidation process also yields sufficient Si−OH surface groups, which are necessary for TEOS-HBA silane attachment.[33] While a complete monolayer coating of silane would serve to further passivate the PSi surface against corrosion, the TEOS-HBA silane tends to form in multilayer islands.[34] Figure 1a shows reflectance spectra taken by prism coupling of an oxidized PSi waveguide after silanization and subsequent soaking in DI water over the course of several hours. The redshift of the waveguide resonance following silanization confirms that silane molecules are attached to the waveguide, whereas the subsequent resonance blueshift after the first 2 h of exposure to DI water indicates a loss of material from the PSi waveguide, likely due to removal of loosely bound silane molecules. After 4 h in DI water, the resonant angle shift stabilized and additional water exposure resulted in negligible shifts in resonance angle (Figure 1b), implying that the remaining silane film is hydrolytically stable.

The fractional coverage of the molecules in the PSi waveguide can be determined by using transfer matrix theory[35] and Lugo's three component effective medium model[36] to fit the magnitude of the resonance angle shifts according to established procedures.[37] Using this method, we found that the shift in resonance angle due to silanization shown in Figure 1, 0.392°, corresponds to a submonolayer surface coverage of approximately 34%. This value should be treated as an upper bound because multilayer islands of silane molecules may still exist on the surface after the annealing and hydrolysis process. According to previous studies on TEOS-HBA silane-functionalized PSi, higher coverages up to nearly 90% can be achieved in PSi waveguides through extended incubation in TEOS-HBA solutions.[34] However, the lower silane coverage was chosen in this work because the surface coverage of silane molecules is directly related to the ensuing probe DNA density in the PSi waveguide and because it has been shown that an approximately 25% probe DNA coverage in PSi waveguides minimizes steric hindrance and results in the largest sensor response on exposure to complementary target oligos.[38] As shown in Figure 2, 16-mer probe DNA synthesis on the silanized PSi waveguides led to a large resonance redshift, confirming molecule attachment. Subsequent deprotection of the DNA probes to give them the structures needed for sensing resulted in a small blueshift, corresponding to the removal of the protecting groups from the DNA chains. On the basis of the overall measured resonance shift of the PSi waveguide resonance due to activated probe DNA attachment (1.113°), the 16-mer probe DNA surface coverage was estimated to be approximately 31%, assuming no corrosion resulted from the attachment process and assuming all sequences were complete 16-mer DNA strands. Absorbance measurements performed on DMT protecting group fractions collected after the first and last base additions in the probe DNA synthesis (Supporting Information, Figure S1) and matrix assisted laser desorption-ionization mass spectrometry (MALDI-MS) measurements performed on fully synthesized DNA 16-mer sequences that were cleaved from the PSi (Supporting Information, Figure S2) suggest a stepwise coupling efficiency of approximately 97% with few failed sequences. The coupling efficiency corresponds well to typical reaction yields reported previously in literature for in situ DNA synthesis in PSi.[39,40] Hence, DNA probes are synthesized from nearly all available silane sites by the in situ synthesis method. We note that the magnitude of the resonance shift from probe DNA attachment is larger than that from silane attachment due to the respective sizes of the molecules (16-mer DNA ≈ 3.52 nm long; TEOS-HBA silane molecule ≈ 0.9 nm long).

The stability of the PSi waveguides functionalized with in situ synthesized probe DNA molecules against corrosion was evaluated by soaking in DI water. Prior studies did not report any corrosion due to the attachment of negatively charged probe DNA molecules,[29] and similar studies performed in our group with presynthesized DNA probes having approximately 10% surface coverage also did not show any measurable

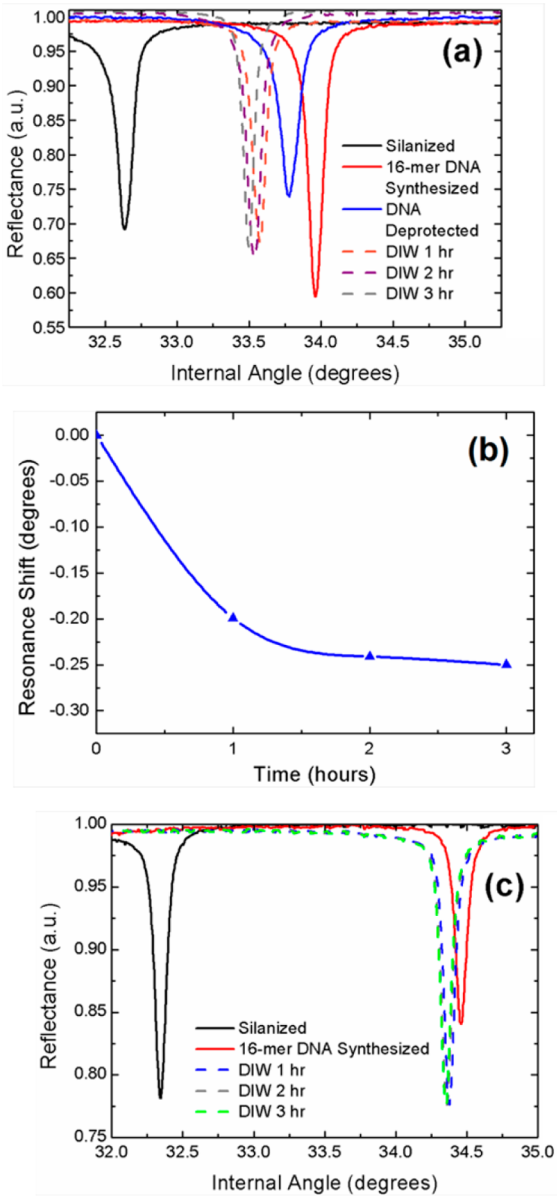

Figure 2. Optical characterization of in situ DNA probe synthesis and subsequent degradation of an activated PSi waveguide biosensor in DI water. (a) Probe DNA was synthesized from a stabilized PSi waveguide functionalized with TEOS-HBA silane (black, solid line). Reflectance spectra following in situ synthesis of 16-mer DNA probe and deprotection of charge-masking groups from the sugar−phosphate backbone are indicated by red and blue solid lines, respectively. Incubation of the deprotected probe DNA molecules with negatively charged backbones in DI water results in a blueshift to lower resonant angles (dashed lines). (b) Resonance angle shift as a function of time during DI water soak after probe DNA deprotection. (c) Reflectance spectra of a PSi waveguide stably functionalized with TEOS-HBA silane (black solid line), after in situ synthesis of probe DNA molecules that have not been deprotected (red solid line), and after soaking the waveguide in DI water (dashed lines).

corrosion effect, likely due to the relatively low concentration of negatively charged species.[41] As shown in Figure 2, a blueshift of the waveguide resonance angle with a magnitude that gradually decreases after the first hour of exposure to DI water was measured, suggesting that the concentration of negative charge provided by the in situ synthesized DNA probes is large enough to lead to measurable corrosion. Because removal of the protecting groups following in situ synthesis leaves the backbone of the probe DNA molecule negatively charged, control experiments on PSi waveguides functionalized with in situ synthesized charge-neutral DNA probes that have not been deprotected could be conducted. Such negative control experiments were performed using protected probe DNA and showed that a smaller waveguide resonance blueshift occurred during the first hour of exposure to DI water and ceased thereafter (Figure 2c). Thus, without deprotection, the charge-neutral DNA probe molecules do not facilitate oxidative corrosion of the PSi surface. From these experiments, we conclude that there may be a small quantity of residual chemicals from the in situ synthesis process or a small quantity of additional incompletely cross-linked silane monomers that are removed during the first hour of DI water exposure to the probe DNA-functionalized PSi waveguides, but there is clearly concurrent and measurable corrosion that occurs due to the presence of the negative charges on the sugar−phosphate backbones of the deprotected DNA probe molecules. Accordingly, to minimize corrosion effects that may potentially mask the binding signal from target DNA molecules during DNA hybridization assays, all in situ DNA probe-functionalized waveguides were stabilized in DI water for at least 2 h after deprotection.

DNA Hybridization with Synthesized DNA Probes. Using the stabilized PSi waveguides with in situ synthesized DNA probes, the effect of corrosion on DNA hybridization was investigated. As shown in Figure 3a, hybridization with 10 μM

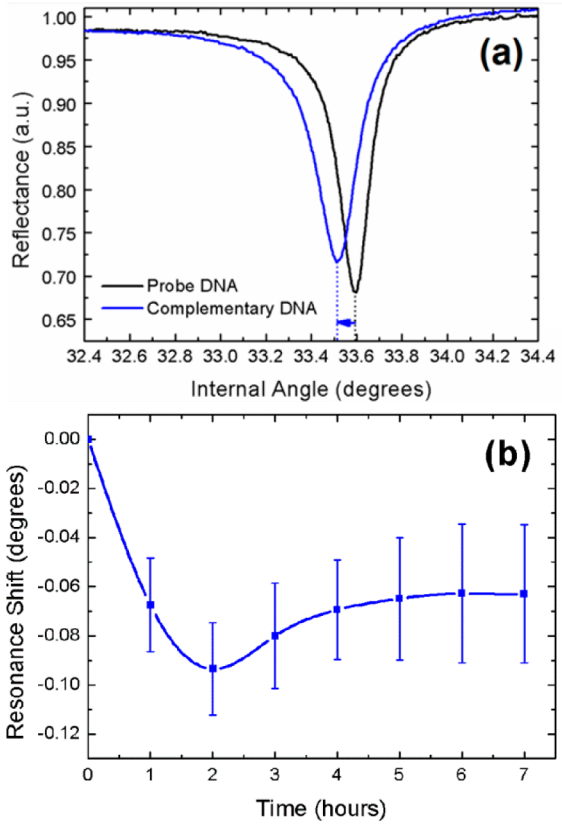

Figure 3. PSi corrosion induced by hybridization with DNA target molecules. (a) Resonance angle blueshift on hybridization of a 100% complementary DNA target (10 μM) with DNA probes synthesized on a PSi waveguide. (b) Resonance angle shift as a function of incubation time with 100% complementary DNA sequence.

complementary DNA target molecules caused the PSi waveguide resonance angle to blueshift approximately 0.1°, suggesting that, even though these waveguides were well-passivated, corrosion of the PSi upon exposure to the DNA duplex occurs.[4,29] Fluorescence measurements using 6-FAM-labeled DNA target molecules (Supporting Information, Figure S3) and FTIR measurements (Supporting Information, Figure S4) were performed to confirm the presence of hybridized DNA duplexes. To verify that the measured blueshift is due to corrosion on DNA hybridization, a 100% mismatch 16-mer DNA sequence was used as a control, and no shift of the resonance angle was detected (Supporting Information, Figure S5). Therefore, the formation of DNA−DNA hybrids at the waveguide surface is necessary for the corrosion observed in Figure 3. As discussed in detail in the Mechanism of Corrosion on Passivated PSi section below, it is possible that the doubling of negative charges due to duplex formation near the PSi waveguide surface, as well as the restricted mobility of the double-stranded compared to single-stranded DNA,[29] enhances the polarization of surface-bound silicon atoms and facilitates nucleophilic attack by water molecules on selected regions that are not perfectly passivated with silane molecules. The role of the DNA surface coverage should also be considered to understand the observed corrosion effect on DNA hybridization in PSi. Previous work reported that ozone oxidized PSi did not exhibit corrosion during DNA hybridization unless the target DNA was labeled with a charge-carrying metal complex;[42] however, the probe DNA coverage in that work was estimated to be 1−2 nmol/cm^2, whereas our probe DNA coverage is estimated to be 1 order of magnitude higher (10−25 nmol/cm^2) due to the in situ DNA synthesis process.

A key distinction in this work compared to a previous study utilizing poorly passivated PSi samples[29] is that the corrosion of the passivated PSi waveguides is not a continuous process that results in complete dissolution of the PSi structure, but rather the extent of corrosion appears to saturate over time. An examination of the time-dependent shift in waveguide resonance angle in Figure 3b reveals that the PSi waveguide resonance ceases to shift to lower angles after 2 h of incubation with complementary DNA targets; a saturating redshift of smaller magnitude than the corrosion-dominated blueshift was observed on further incubation. These shifts suggest that PSi corrosion initially occurs at a rate fast enough to mask DNA binding events. As the corrosion progresses, the corrosion rate appears to slow, similar to what was observed on in situ synthesized probe DNA attachment, and a resonance redshift can be observed due to continued target DNA binding. However, the overall PSi waveguide resonance shift due to target DNA binding is to a smaller angle, indicating that the corrosion effect would dominate the measured transduction signal for DNA sensor applications when well-passivated PSi waveguide sensors are functionalized with DNA probe molecules.

Because the doubling of negative charges on the surface during hybridization increases corrosion, it is expected that, in general, PSi corrosion is enhanced with increasing target DNA concentration. As shown in Figure 4, a study of the effect of DNA target concentration on PSi corrosion after 1 h exposure reveals that the corrosion level on passivated PSi waveguides increases with DNA target concentration, reaching a saturation as evidenced by no additional resonance blueshift for concentrations above approximately 10 μM. As the target DNA concentration reaches this threshold value, most of the

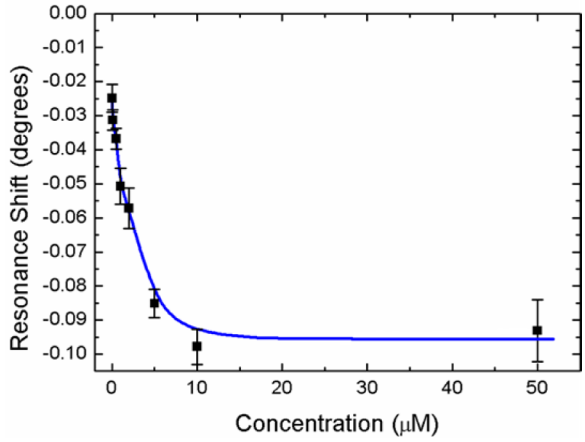

Figure 4. Dependence of PSi biosensor corrosion on target DNA concentration. Waveguide resonance blueshift on 1 h incubation with 100% complementary DNA sequence at different concentrations. The line is shown as a guide to the eye.

accessible probe DNA molecules have been hybridized by complementary DNA targets within the 1 h measurement. Hence, both the resonance blueshift, which is likely due to corrosion of exposed Si−OH bonds as discussed in the Mechanism of Corrosion on Passivated PSi section, and the resonance redshift due to target DNA attachment saturate.

DNA Hybridization with Synthesized PNA Probes. DNA hybridization and PSi corrosion can happen simultaneously, and the redshift resulting from target DNA binding can therefore be obscured by the blueshift resulting from corrosion. This obscurity must be eliminated in order to quantitatively determine molecule infiltration into PSi. One possible strategy for preventing PSi surface corrosion during functionalization and minimizing the corrosion during target DNA hybridization is to replace DNA probes with neutrally charged PNA probes. In this way, a smaller concentration of negative charge attaches to the functionalized PSi surface during target DNA capture. Meanwhile, due to its uncharged polyamide backbone, PNA can hybridize to negatively charged DNA without electrostatic repulsion, which increases the rate of hybridization and binding affinity.[43,44] As a direct analog of the in situ synthesis method of growing DNA probe molecules base-by-base inside the PSi waveguide, a recently developed method of in situ probe PNA synthesis was employed in PSi waveguides.[32] On the basis of the magnitude of the resulting waveguide resonance shift, a similar surface coverage of probe PNA molecules (≈28%) as compared with that of DNA molecules (≈31%) was achieved after PNA synthesis and deprotection. We note that this estimated 16-mer probe PNA coverage is an upper bound, as the stepwise coupling efficiency was found to be 92%, suggesting the presence of some failed sequences that would also contribute to the resonance shift (Supporting Information, Figure S6). Soaking the PNA probe functionalized PSi waveguide sample in DI water yielded a small blueshift that saturated after 1 h (−0.061°), similar to that observed when the PSi waveguide functionalized with protected, neutrally charged, DNA probes was soaked in DI water (Supporting Information, Figure S7). This suggests that no oxidative corrosion occurs on the probe PNA-functionalized PSi structure. Figure 5a shows that a waveguide resonance redshift of 0.068° was observed after 1 h incubation of the PNA-functionalized PSi sample with 10 μM complementary

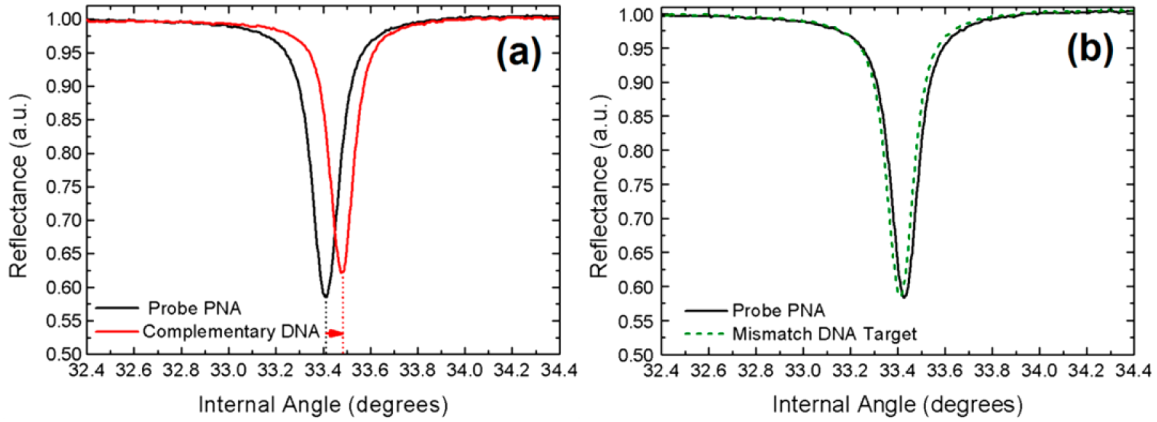

Figure 5. Functionalization of PSi waveguide surface with neutrally charged PNA probes mitigates waveguide corrosion during hybridization with DNA targets. Resonance shifts are shown for a PNA probe-functionalized PSi waveguide on incubation with (a) 100% complementary DNA sequence and (b) 100% mismatch DNA sequence.

DNA in HEPES buffer. Hence, the dominant effect is clearly PNA–DNA hybridization. As a control, a negligible shift was observed after incubation with a 100% mismatch DNA sequence (Figure 5b).

In order to determine whether corrosion still occurs during DNA hybridization to PNA probes, we conducted an experiment in which PNA target molecules were hybridized to in situ synthesized PNA probe molecules in a passivated PSi waveguide. In this case, no negative charges are present, and the only effect on the waveguide resonance shift is the material addition due to PNA attachment. Figure 6 shows that a

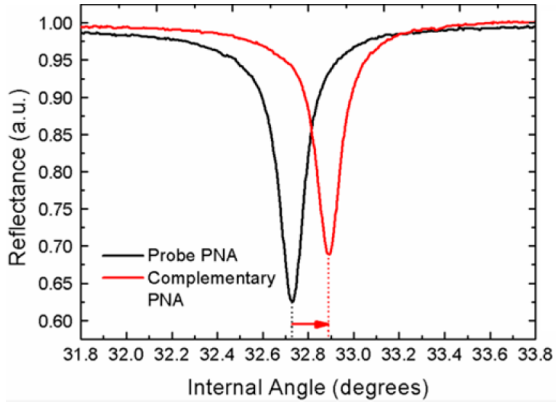

Figure 6. Resonance shift for a PNA probe-functionalized PSi waveguide on incubation with 100% complementary PNA oligo target.

waveguide resonance redshift of 0.152° was observed after 1 h incubation of the PNA-functionalized PSi sample with 10 μM complementary PNA in DI water. The PNA–PNA duplex has a rise per base pair of 3.2 Å, similar to the rise per base pair in a PNA–DNA helix (3.5 Å); however, the PNA–PNA duplex is a wider helix, with a diameter of 28 Å compared to the PNA–DNA helix that has a diameter of 22 Å.[45,46] Considering the respective sizes of PNA–DNA and PNA–PNA hybrids, if no corrosion effect occurs during PNA–DNA hybridization, then the redshift observed for target PNA attachment would be about 1.5 times larger than the redshift observed for target DNA attachment, corresponding to a PNA–PNA hybridization redshift of approximately 0.10°. However, because the measured resonance redshift for PNA–PNA hybridization (0.152°) was larger than this value, we concluded that even with utilization of a charge-neutral PNA probe molecule, DNA sensing in PSi is still challenged by corrosion during the hybridization of the negatively charged DNA molecules. Note that for both PNA–DNA binding and PNA–PNA binding relatively low hybridization efficiencies were observed, likely due to size-dependent molecular infiltration challenges for the target molecules.[47] If all of the probe PNA molecules capture target PNA molecules, then a resonance shift of nearly equal magnitude to that shown by the waveguide after probe PNA attachment would be observed (Supporting Information, Figure S7), whereas if all probe PNA molecules capture DNA targets, then a 1.5 times smaller magnitude resonance shift compared to that shown by the waveguide after probe PNA attachment would result. While a nonambiguous waveguide resonance redshift is observed for target DNA hybridization to probe PNA molecules, the overall response of the sensor is still compromised by the concurrent blueshift that occurs due to corrosion. Therefore, the sensitivity of the sensor is also compromised by the corrosion effect.

Compensating DNA Charge with Magnesium. In order to more completely shield the PSi surface from the negative charges on the phosphate groups of the target DNA molecules and to fully mitigate DNA-induced corrosion of PSi, Mg^{2+} ions were introduced into the incubation solution used for target molecule hybridization with synthesized PNA probes, following results reported in ref 29. Mg^{2+} ions have a positive two charge; thus, when binding to the DNA strands, they can shield the negative charge accumulated at the PSi surface more effectively than cations with a single positive charge, such as Na^+ and K^+.[48,49] Shielding of the negative charges accumulated at the PSi surface prevents PSi corrosion and enhances the detection signal for the PNA-functionalized PSi waveguide, as shown by the increased magnitude of the waveguide resonance redshift from 0.068° (no $MgCl_2$ in buffer, Figure 5a) to 0.107° (2 M $MgCl_2$ in buffer, Figure 7a) on hybridization with 10 μM 100% complementary target DNA molecules after 1 h incubation. The magnitude of the redshift observed after DNA hybridization in the presence of Mg^{2+} ions is about 1.4 times smaller than the sensing results with PNA hybridization, which is consistent with the respective sizes of the PNA–DNA and PNA–PNA helixes and suggests that the Mg^{2+} ions effectively mitigate the DNA-induced corrosion process during hybridization. A negligible resonance shift was detected for mismatch DNA target in the same buffer solution with Mg^{2+}, suggesting

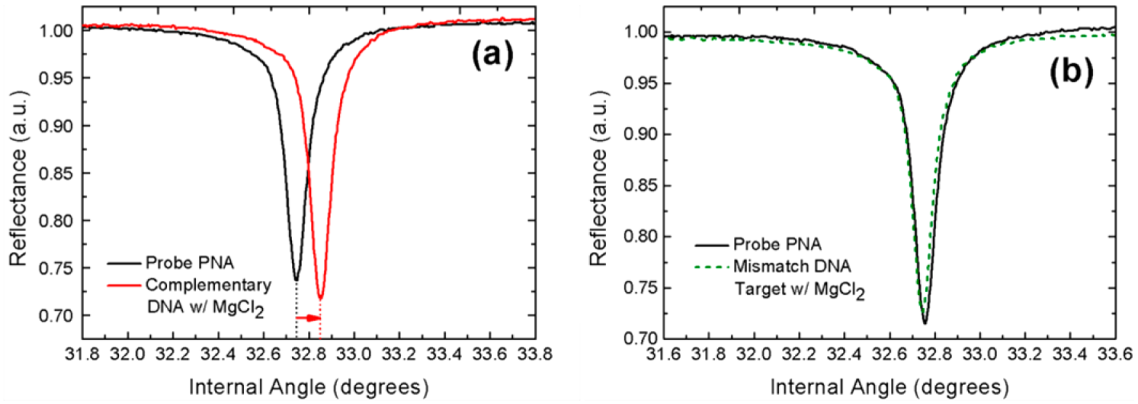

Figure 7. Addition of Mg^{2+} ions mitigates PSi waveguide corrosion during hybridization of DNA targets to PNA probes. Resonance shifts are shown on incubation with (a) 100% complementary DNA and (b) 100% mismatch DNA in the presence of 2 M $MgCl_2$.

there are no nonspecific binding events (Figure 7b). In other work, we have shown that a passivated PSi waveguide biosensor similar to the one studied in this work can achieve a detection limit near 10 nM.[41] Although a detection limit near 0.1 nM was reported for a PSi single-layer biosensor based on exploitation of the corrosion effect with a poorly passivated film,[29] the repeatability and reliability of the sensing results are sacrificed using this corrosion-based transduction approach.

Mechanism of Corrosion on Passivated PSi. On the basis of the experimental measurements characterizing the effect of corrosion in PSi waveguides, we propose a model in which the corrosion in PSi waveguides depends on the surface charge density and passivation conditions of the PSi structures. When the surface coverage of the immobilized DNA molecules increases, the amount of negative charge associated with DNA increases as well. The accumulation of negative charges near the PSi surface attracts the majority carriers of *p*-type PSi to move to the vicinity of the DNA binding event, which enhances the localized electric field near the DNA−oxide interface. This electric field may promote further oxidation of the Si pore wall and result in a blueshift of the PSi waveguide reflectance spectrum. However, an enhanced electric field is unlikely the main reason for the PSi corrosion that is experimentally observed as the increased silicon oxidation rate reported previously in literature requires an applied electric field of approximately 10^4 V/cm with a high temperature of 850 °C,[50] which is not applicable to the PSi DNA sensors studied in this work. Another possible explanation for PSi corrosion is the electrical double layer, with one polar component of the electrolyte being preferentially accumulated at the electrode surface and in the diffuse layer while the other polar component is depleted in the same region.[51] The electrical double layer was reported to accelerate the wet etching of SiO_2 by locally increasing the concentration of hydroxide around a hydrophobic carbon nanotube.[52] However, electric double layer formation is also not likely the predominant reason for the observed corrosion effect because a hydrophilic, thermally oxidized PSi surface functionalized with silane molecules and negatively charged DNA strands cannot adsorb the high effective concentration of hydroxide that would be necessary to accelerate SiO_2 etching. According to a previously proposed mechanism for DNA hybridization enhanced corrosion, which is the most likely cause of PSi corrosion, the accumulation of negatively charged DNA near the PSi surface enhances the polarization of surface silicon bonds and facilitates nucleophilic attack by water molecules starting at exposed Si−H bonds.[29] As shown in Figure 8, the FTIR spectrum of a freshly etched PSi waveguide showed strong reflectance in the region from 2038

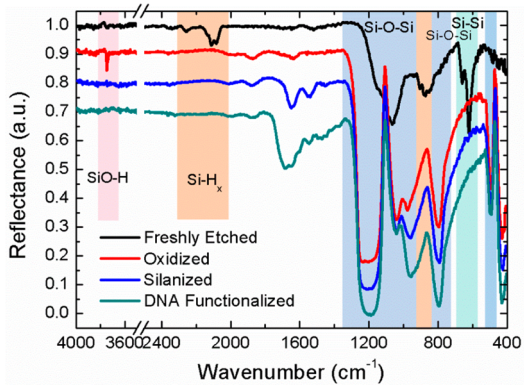

Figure 8. FTIR spectra of PSi waveguide freshly etched, oxidized at 800 °C for 30 min, silanized with TEOS-HBA silane, and functionalized with deprotected 16-mer DNA probes.

to 2280 cm^{-1} and at 900 cm^{-1}, attributed to Si−H_x (x = 1, 2, 3) groups on the surface. After thermal oxidation at 800 °C for 30 min, PSi waveguide samples showed FTIR spectral signatures for Si−O−Si bonds from 900 to 1300 and 800 cm^{-1}, and the isolated SiO−H stretching at 3750 cm^{-1}.[33] The spectral band representing Si−Si bonding near 620 cm^{-1} as well as the bands for Si−H_x bonds disappear after oxidation, indicating that the PSi waveguide structure has been well-oxidized. Because of the low sensitivity of the IR measurement, it is not possible to confirm complete oxidation of the PSi waveguide surface based on the disappearance of Si−Si and Si−H_x bands. Disappearance of the Si−H_x groups after thermal oxidation, however, does indicate good passivation of the PSi waveguide surface. The Si−H bond is a reducing agent and is susceptible to nucleophilic attack by water. Oxidation first turns the surface silicon atoms into Si−OH bonds. Further oxidation results in condensation of neighboring surface Si−OH bonds, forming Si−O−Si bridges, which contribute to passivation of the PSi surface.[53] Following silanization, the FTIR spectrum shows characteristic peaks for triethoxysilane in the region around 1595 cm^{-1}. The isolated peak at 3750 cm^{-1} for SiO−H disappears after silane attachment. The region of PSi covered by silane is well-passivated by a covalent Si−O−Si bonding pattern on the surface; however, any remaining Si−OH bonds on PSi surface are susceptible to nucleophilic attack by water molecules. After

Scheme 1. Schematic of the DNA-Induced Corrosion Process in PSi Illustrating Surface Regions of the Waveguide Structure[a]

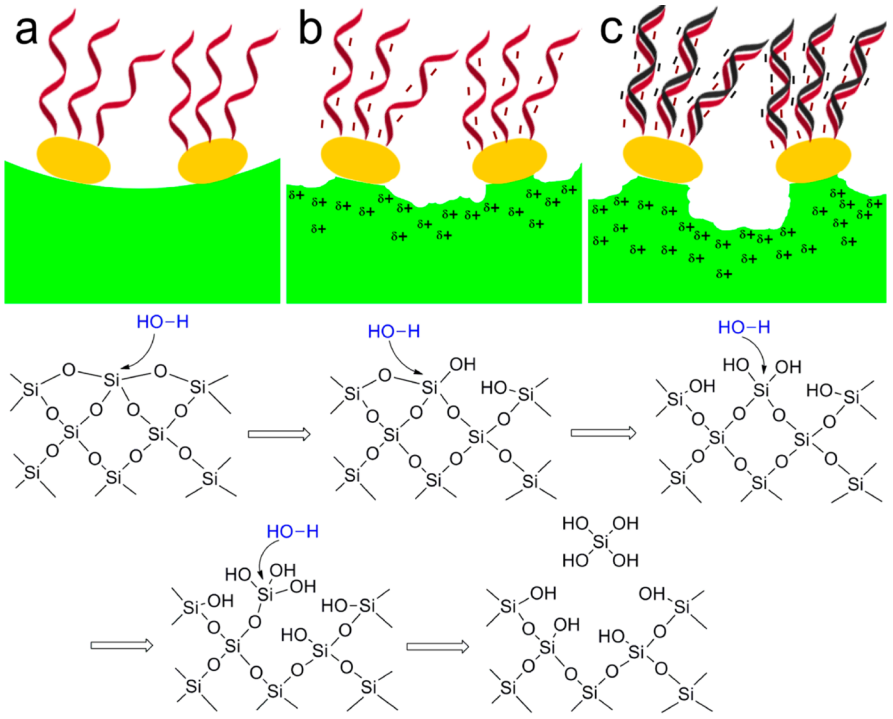

[a]The green region indicates the thermal oxide on pore walls; the yellow represents silane molecules; DNA oligos are represented by the red (probe) and black (target) helix structures attached on the silane molecules. The chemical reactions present a possible mechanism for corrosion of a silicon atom initiated by sequential nucleophilic attacks by water molecules and resulting in the release and dissolution of the atom in the form of $Si(OH)_4$.

in situ synthesis of 16-mer DNA molecules, characteristic peaks for DNA appears in the region from 1500 to 1800 cm^{-1}.

The presence of Si–O–Si bonds at the PSi waveguide surface even after synthesis of DNA probes provides a mechanism for the DNA-induced corrosion observed throughout this study. We propose the following scheme for DNA-induced corrosion of PSi waveguides passivated with thermal oxide, TEOS-HBA silane, and in situ synthesized probe DNA molecules. Before deprotection, a cyanoethyl group masks the negative charges on the probe DNA backbones (Scheme 1a). Following deprotection, the corrosion process initiates at Si–O–Si bonds adjacent to immobilized DNA probes (Scheme 1b). During hybridization, the local concentration of negative charges in the PSi matrix increases due to target DNA binding (Scheme 1c). The increased concentration of negative charges enhances the corrosion rate of the PSi surface in regions that are not passivated by silane and PNA/DNA molecules. Si–O bonds on oxidized PSi surfaces are highly polarized and thus are susceptible to nucleophilic attack, according to the reaction equations in Scheme 1.

Negatively charged DNA at the surface enhances the polarization of silicon bonds; therefore, positive charges in *p*-type PSi accumulate near the surface where DNA binding events occur. The resulting highly polarized and reactive surface-bound silicon atoms are prone to chemical attack by water molecules, leading to accelerated corrosion of PSi. On poorly passivated PSi samples, the low energy required to break Si–H and Si–Si bonds (bond energies of 318 and 197 kJ/mol, respectively) leads to continued corrosion. In the case of well-passivated PSi, the blueshift of the resonance angle resulting from corrosion was most pronounced during the first 2 h of incubation. The corrosion rate slows for longer incubation times, as the energy required to break Si–O bonds with average bond energy of 368 kJ/mol is higher than that required to break Si–H and Si–Si bonds. When the corrosion progresses deeper into the pore walls and reaches the underlying Si–O–Si bridges formed during thermal oxidation, the polarization enhancement of silicon bonds resulting from negatively charged DNA on the surface ceases, making nucleophilic attack toward Si atoms by water molecules more difficult and preventing continued corrosion of PSi. Thus, the corrosion process for passivated PSi waveguide samples was observed to saturate over time. Importantly, this saturation of the corrosion process allows reusability of the passivated PSi sensor. In this work, the PSi waveguide sensor was reused for DNA detection after denaturing the DNA–DNA or DNA–PNA duplex structures in DI water at 70 or 95 °C for 30 s. After denaturing, the DNA/PNA probes remained active for the next hybridization event, while the target molecules were unbound from the probes. The PSi waveguide sensors can be reused at least five times and maintain stability and reproducibility of the sensing results. Ultimately, the lifetime of these passivated PSi sensors is likely to be limited by activity retention of probe DNA/PNA molecules as well as degradation of both silane molecules and the PSi network that may occur on repeated usage of the sensors.

CONCLUSIONS

Charge density and surface passivation of PSi play significant roles in the accuracy, sensitivity, and stability of PSi-based biosensors. When the amount of negative charges immobilized in the PSi matrix increases, the polarization of silicon bonds on the PSi surface is enhanced, facilitating nucleophilic attack of silicon atoms by water molecules. This corrosion process is highly charge-dependent, as both increased DNA probe density

and increased DNA target concentration led to a blueshift of the waveguide resonance angle. Corrosion can be partially mitigated by replacing the DNA probe with charge-neutral PNA or fully mitigated by additionally introducing Mg^{2+} ions to shield negative charges on the target DNA backbone during hybridization to the PNA probes. Through these methods, the signal ambiguity for PSi-based DNA sensing can be overcome, and repeatable DNA sensing results can be achieved. PSi waveguide biosensors in this study were reused at least five times without sacrificing sensitivity or specificity. Further improvement in PSi passivation, perhaps with the implementation of a mixed silane approach using reactive and nonreactive components that allow for a more complete silane surface passivation while maintaining a moderate probe density coverage, may eliminate PSi corrosion even without the need for Mg^{2+} ions and further increase the robustness of PSi DNA sensors.

■ ASSOCIATED CONTENT

Supporting Information

Detailed experimental methods and results for absorbance measurements of DMT collected during in situ DNA synthesis and mass spectrometry of in situ synthesized DNA cleaved from PSi. Fluorescence spectrum of PSi waveguide functionalized with in situ synthesized probe DNA molecules after hybridization with fluorescently labeled complementary DNA. FTIR spectra for a probe DNA-functionalized PSi waveguide before and after hybridization with complementary DNA. Reflectance spectra of an in situ probe DNA-functionalized PSi waveguide on exposure to a 100% mismatch DNA sequence. Absorbance measurement of Fmoc protecting groups collected during in situ PNA synthesis. Reflectance spectra of PSi waveguide functionalized with 3-APTES silane and in situ synthesized probe PNA molecules before and after soaking the waveguide in DI water. This material is available free of charge via the Internet at http://pubs.acs.org.

■ AUTHOR INFORMATION

Corresponding Author

*E-mail: sharon.weiss@vanderbilt.edu. Tel: +1-615-343-8311. Fax: +1-615-343-6702.

Present Address

[‖]Webb School of Knoxville, 9800 Webb School Lane, Knoxville, Tennessee 37923, United States.

Notes

The authors declare no competing financial interest.

■ ACKNOWLEDGMENTS

This work was supported in part by the Army Research Office (W911NF-09-1-0101). The authors gratefully acknowledge G. Gaur, S. Hu, G. A. Rodriguez, K. Qin, and Dr. Y. Jiao for useful discussions and technical assistance. The authors would also like to thank Dr. J. W. Mares and M. L. Reyzer for providing assistance with and access to MALDI-MS at the Mass Spectrometry Research Center at Vanderbilt University. FTIR spectroscopy and scanning electron microscopy were performed at the Vanderbilt Institute of Nanoscale Science and Engineering. K.R.B. acknowledges funding from an NSF Graduate Fellowship.

■ REFERENCES

(1) Sailor, M. J. *Porous Silicon in Practice: Preparation, Characterization and Applications*; Wiley-VCH: Weinheim, Germany, 2011; Chapter 1, pp 1−42.

(2) Stewart, M. P.; Buriak, J. M. Chemical and Biological Applications of Porous Silicon Technology. *Adv. Mater.* **2000**, *12*, 859−869.

(3) Sailor, M. J. Color Me Sensitive: Amplification and Discrimination in Photonic Silicon Nanostructures. *ACS Nano* **2007**, *1*, 248−252.

(4) Lin, V. S. Y.; Motesharei, K.; Dancil, K. P. S.; Sailor, M. J.; Ghadiri, M. R. A Porous Silicon-Based Optical Interferometric Biosensor. *Science* **1997**, *278*, 840−843.

(5) Janshoff, A.; Dancil, K.-P. S.; Steinem, C.; Greiner, D. P.; Lin, V. S. Y.; Gurtner, C.; Motesharei, K.; Sailor, M. J.; Ghadiri, M. R. Macroporous P-Type Silicon Fabry−Perot Layers. Fabrication, Characterization, and Applications in Biosensing. *J. Am. Chem. Soc.* **1998**, *120*, 12108−12116.

(6) Gruning, U.; Lehmann, V.; Engelhardt, C. M. Two-Dimensional Infrared Photonic Band Gap Structure Based on Porous Silicon. *Appl. Phys. Lett.* **1995**, *66*, 3254−3256.

(7) Gruning, U.; Lehmann, V.; Ottow, S.; Busch, K. Macroporous Silicon with a Complete Two-Dimensional Photonic Band Gap Centered at 5 μm. *Appl. Phys. Lett.* **1996**, *68*, 747−749.

(8) Birner, A.; Wehrspohn, R. B.; Gosele, U. M.; Busch, K. Silicon-Based Photonic Crystals. *Adv. Mater.* **2001**, *13*, 377−388.

(9) Wolkin, M. V.; Jorne, J.; Fauchet, P. M.; Allan, G.; Delerue, C. Electronic States and Luminescence in Porous Silicon Quantum Dots: The Role of Oxygen. *Phys. Rev. Lett.* **1999**, *82*, 197−200.

(10) Aravamudhan, S.; Rahman, A. R. A.; Bhansali, S. Porous Silicon Based Orientation Independent, Self-Priming Micro Direct Ethanol Fuel Cell. *Sens. Actuators, A* **2005**, *123−124*, 497−504.

(11) Shin, H.-C.; Corno, J. A.; Gole, J. L.; Liu, M. Porous Silicon Negative Electrodes for Rechargeable Lithium Batteries. *J. Power Sources* **2005**, *139*, 314−320.

(12) Kemell, M.; Ritala, M.; Leskelä, M.; Ossei-Wusu, E.; Carstensen, J.; Föll, H. $Si/Al_2O_3/ZnO$:Al Capacitor Arrays Formed in Electrochemically Etched Porous Si by Atomic Layer Deposition. *Microelectron. Eng.* **2007**, *84*, 313−318.

(13) Jane, A.; Dronov, R.; Hodges, A.; Voelcker, N. H. Porous Silicon Biosensors on the Advance. *Trends Biotechnol.* **2009**, *27*, 230−239.

(14) Ouyang, H.; Christophersen, M.; Viard, R.; Miller, B. L.; Fauchet, P. M. Macroporous Silicon Microcavities for Macromolecule Detection. *Adv. Funct. Mater.* **2005**, *15*, 1851−1859.

(15) Saarrinen, J. J.; Weiss, S. M.; Fauchet, P. M.; Sipe, J. E. Optical Sensor Based on Resonant Porous Silicon Structures. *Opt. Express* **2005**, *13*, 3754−3764.

(16) Stefano, L. D.; Rotiroti, L.; Rea, I.; Moretti, L.; Francia, G. D.; Massera, E.; Lamberti, A.; Arcari, P.; Sanges, C.; Rendina, I. Porous Silicon-Based Optical Biochips. *J. Opt. A: Pure Appl. Opt.* **2006**, *8*, S540−S544.

(17) Rong, G.; Najmaie, A.; Sipe, J. E.; Weiss, S. M. Nanoscale Porous Silicon Waveguide for Label-Free DNA Sensing. *Biosens. Bioelectron.* **2008**, *23*, 1572−1576.

(18) Cullis, A. G.; Canham, L. T.; Calcott, P. D. J. The Structural and Luminescence Properties of Porous Silicon. *J. Appl. Phys.* **1997**, *82*, 909−965.

(19) Theiß, W. Optical Properties of Porous Silicon. *Surf. Sci. Rep.* **1997**, *29*, 91−192.

(20) Buriak, J. M. Organometallic Chemistry on Silicon and Germanium Surfaces. *Chem. Rev.* **2002**, *102*, 1271−1308.

(21) Kilian, K. A.; Böcking, T.; Ilyas, S.; Gaus, K.; Jessup, W.; Gal, M.; Gooding, J. J. Forming Antifouling Organic Multilayers on Porous Silicon Rugate Filters Towards in Vivo/ex Vivo Biophotonic Devices. *Adv. Funct. Mater.* **2007**, *17*, 2884−2890.

(22) Collins, B. E.; Dancil, K. P. S.; Abbi, G.; Sailor, M. J. Determining Protein Size Using an Electrochemically Machined Pore Gradient in Silicon. *Adv. Funct. Mater.* **2002**, *12*, 187−191.

(23) Bayliss, S. C.; Heald, R.; Fletcher, D. I.; Buckberry, L. D. The Culture of Mammalian Cells on Nanostructured Silicon. *Adv. Mater.* **1999**, *11*, 318−321.
(24) Alvarez, S. D.; Derfus, A. M.; Schwartz, M. P.; Bhatia, S. N.; Sailor, M. J. The Compatibility of Hepatocytes with Chemically Modified Porous Silicon with Reference to in Vitro Biosensors. *Biomaterials* **2009**, *30*, 26−34.
(25) Bonanno, L. M.; DeLouise, L. A. Whole Blood Optical Biosensor. *Biosens. Bioelectron.* **2007**, *23*, 444−448.
(26) Gowda, S. R.; Pushparaj, V.; Herle, S.; Girishkumar, G.; Gordon, J. G.; Gullapalli, H.; Zhan, X.; Ajayan, P. M.; Reddy, A. L. M. Three-Dimensionally Engineered Porous Silicon Electrodes for Li Ion Batteries. *Nano Lett.* **2012**, *12*, 6060−6065.
(27) Oakes, L.; Westover, A.; Mares, J. W.; Chatterjee, S.; Erwin, W. R.; Bardhan, R.; Weiss, S. M.; Pint, C. L. Surface Engineered Porous Silicon for Stable, High Performance Electrochemical Supercapacitors. *Sci. Rep.* **2013**, *3*.
(28) Dancil, K.-P. S.; Greiner, D. P.; Sailor, M. J. A Porous Silicon Optical Biosensor: Detection of Reversible Binding of IgG to a Protein A-Modified Surface. *J. Am. Chem. Soc.* **1999**, *121*, 7925−7930.
(29) Steinem, C.; Janshoff, A.; Lin, V. S. Y.; Völcker, N. H.; Ghadiri, M. R. DNA Hybridization-Enhanced Porous Silicon Corrosion: Mechanistic Investigations and Prospect for Optical Interferometric Biosensing. *Tetrahedron* **2004**, *60*, 11259−11267.
(30) Lawrie, J. L.; Xu, Z.; Rong, G.; Laibinis, P. E.; Weiss, S. M. Synthesis of DNA Oligonucleotides in Mesoporous Silicon. *Phys. Status Solidi A* **2009**, *206*, 1339−1342.
(31) Böcking, T.; Kilian, K. A.; Gaus, K.; Gooding, J. J. Modifying Porous Silicon with Self-Assembled Monolayers for Biomedical Applications: The Influence of Surface Coverage on Stability and Biomolecule Coupling. *Adv. Funct. Mater.* **2008**, *18*, 3827−3833.
(32) Beavers, K. R.; Mares, J. W.; Swartz, C. M.; Zhao, Y.; Weiss, S. M.; Duvall, C. L. In Situ Synthesis of Peptide Nucleic Acids in Porous Silicon for Drug Delivery and Biosensing. *Bioconjugate Chem.* **2014**, *25*, 1192−1197.
(33) Riikonen, J.; Salomäki, M.; van Wonderen, J.; Kemell, M.; Xu, W.; Korhonen, O.; Ritala, M.; MacMillan, F.; Salonen, J.; Lehto, V.-P. Surface Chemistry, Reactivity, and Pore Structure of Porous Silicon Oxidized by Various Methods. *Langmuir* **2012**, *28*, 10573−10583.
(34) Lawrie, J. L.; Weiss, S. M. Stabilization of Hydroxyl-Terminated Silanes in Porous Silicon for in-Situ DNA Synthesis. *Phys. Status Solidi C* **2011**, *8*, 1851−1855.
(35) Yeh, P. *Optical Waves in Layered Media*; Wiley: Hoboken, NJ, 1988; Chapter 5, pp 102−114.
(36) Lugo, J. E.; Lopez, H. A.; Chan, S.; Fauchet, P. M. Porous Silicon Multilayer Structures: A Photonic Band Gap Analysis. *J. Appl. Phys.* **2002**, *91*, 4966−4972.
(37) Jiao, Y.; Weiss, S. M. Design Parameters and Sensitivity Analysis of Polymer-Cladded Porous Silicon Waveguides for Small Molecule Detection. *Biosens. Bioelectron.* **2010**, *25*, 1535−1538.
(38) Rodriguez, G. A.; Lawrie, J. L.; Weiss, S. M. In *Porous Silicon for Biomedical Applications*, 1st ed.; Santos, H. A., Ed.; Woodhead Publishing Ltd.: Sawston, Cambridge, 2014; Chapter 13, pp 324−326.
(39) McInnes, S. J.; Voelcker, N. Porous Silicon-Based Nanostructured Microparticles as Degradable Supports for Solid-Phase Synthesis and Release of Oligonucleotides. *Nanoscale Res. Lett.* **2012**, *7*, 385−395.
(40) Rea, I.; Oliviero, G.; Amato, J.; Borbone, N.; Piccialli, G.; Rendina, I.; De Stefano, L. Direct Synthesis of Oligonucleotides on Nanostructured Silica Multilayers. *J. Phys. Chem. C* **2010**, *114*, 2617−2621.
(41) Zhao, Y.; Lawrie, J. L.; Laibinis, P. E.; Weiss, S. M. Understanding and Mitigating DNA Induced Corrosion in Porous Silicon Based Biosensors. *Proc. SPIE* **2014**, *8933*, 893302−893309.
(42) Voelcker, N. H.; Alfonso, I.; Ghadiri, M. R. Catalyzed Oxidative Corrosion of Porous Silicon Used as an Optical Transducer for Ligand−Receptor Interactions. *ChemBioChem.* **2008**, *9*, 1776−1786.
(43) Nielsen, P. E.; Egholm, M. An Introduction to Peptide Nucleic Acid. *Curr. Issues Mol. Biol.* **1999**, *1*, 89−104.
(44) Ratilainen, T.; Holmén, A.; Nordén, B. In *Peptide Nucleic Acids: Protocols and Applications*, 2nd ed.; Nielsen, P. E., Ed.; Horizon Bioscience: Wymondham, U.K., 2004; Chapter 4, pp 93−96.
(45) Menchise, V.; De Simone, G.; Tedeschi, T.; Corradini, R.; Sforza, S.; Marchelli, R.; Capasso, D.; Saviano, M.; Pedone, C. Insights into Peptide Nucleic Acid (PNA) Structural Features: The Crystal Structure of a D-Lysine-Based Chiral PNA−DNA Duplex. *Proc. Natl. Acad. Sci. U.S.A.* **2003**, *100*, 12021−12026.
(46) Rasmussen, H.; Sandholm, J. Crystal Structure of a Peptide Nucleic Acid (PNA) Duplex at 1.7 Angstrom Resolution. *Nat. Struct. Biol.* **1997**, *4*, 98−101.
(47) Lawrie, J. L.; Yang, J.; Weiss, S. M. Size-Dependent Infiltration and Optical Detection of Nucleic Acids in Nanoscale Pores. *IEEE Trans. Nanotechnol.* **2010**, *9*, 596−602.
(48) Todd, B. A.; Rau, D. C. Interplay of Ion Binding and Attraction in DNA Condensed by Multivalent Cations. *Nucleic Acids Res.* **2007**, *36*, 501−510.
(49) Keyser, U. F.; Koeleman, B. N.; van Dorp, S.; Krapf, D.; Smeets, R. M. M.; Lemay, S. G.; Dekker, N. H.; Dekker, C. Direct Force Measurements on DNA in a Solid-State Nanopore. *Nat. Phys.* **2006**, *2*, 473−477.
(50) Jorgensen, P. J. Effect of an Electric Field on Silicon Oxidation. *J. Chem. Phys.* **1962**, *37*, 874−877.
(51) Lauw, Y.; Horne, M. D.; Rodopoulos, T.; Nelson, A.; Leermakers, F. A. M. Electrical Double-Layer Capacitance in Room Temperature Ionic Liquids: Ion-Size and Specific Adsorption Effects. *J. Phys. Chem. B* **2010**, *114*, 11149−11154.
(52) Liu, H.; Steigerwald, M. L.; Nuckolls, C. Electrical Double Layer Catalyzed Wet-Etching of Silicon Dioxide. *J. Am. Chem. Soc.* **2009**, *131*, 17034−17035.
(53) Zhang, X. G. *Electrochemistry of Silicon and Its Oxide*; Kluwer Academic/Plenum Publishers: New York, 2001; Chapter 5, p 199.